CHEMSUSCHEM

DOI: 10.1002/cssc.201000322

Nanostructured Carbon–Metal Oxide Hybrids as Amphiphilic Emulsion Catalysts

M. Pilar Ruiz, Jimmy Faria, Min Shen, Santiago Drexler, Teerawit Prasomsri, and Daniel E. Resasco*[a]

Nanohybrids composed of "onion-like" carbon, single-walled (SWCNTs) or multi-walled carbon nanotubes (MWCNTs) fused to silica or alumina particles have been compared as stabilizers of water/oil emulsions and interfacial catalysts. The amphiphilic character of these nanohybrids makes them effective in stabilizing emulsions (up to 85% of total volume) comprising of small droplets (less than 40 μm). Furthermore, these nanohybrids have been used as supports for transition metal particles (palladium and copper) to catalyze reactions at the water/oil interface. Three different reaction systems have been conducted in the emulsions to demonstrate the principle: 1) hydrogenation of phenanthrene; 2) hydrogenation of glutaraldehyde and benzaldehyde; 3) oxidation of tetralin. Comparison of the maximum conversions achieved in emulsions as opposed to the single phase, together with much better control of selectivity in the two-phase system shows the benefits of using these nanohybrid catalysts.

Introduction

Since the discovery of the carbon nanotube (CNT),[1] extended efforts have been made to understand their outstanding physical, chemical, mechanical, and electrical properties,[2–7] to develop applications, and to expand production scale.[8,9] The controlled synthesis of both single-walled (SWCNTs) and multi-walled carbon nanotubes (MWCNTs) has generated a vast number of studies dedicated to the development of applications in many fields, including nanocomposites, sensors, electronics, field emission, thin films, catalysis, and energy storage.[10–14] Specifically, in the field of heterogeneous catalysis, CNTs have been used as catalytic materials,[15–18] catalyst supports,[19] and catalyst promoters.[20] Nanotubes exhibit several promising features for catalysis including very high surface area, high resistance to temperature in non-oxidizing environments, and acidic and basic environments, as well as surface reactivity and chemical tunability, achieved by functionalization.

We recently reported a study on the application of amphiphilic nanohybrid particles, based on CNTs fused to metal oxides, as recoverable emulsion stabilizers and catalyst supports to use in water/oil interfaces.[21] The amphiphilic character of these nanohybrids, which derives from the combination of hydrophobic CNTs and hydrophilic metal oxides, favored the stabilization of Pickering emulsions in water/oil systems.[22] Similar studies have been conducted by other research groups.[19]

Pristine CNTs are known to be hydrophobic,[23,24] but, at the same time, they cannot be effectively suspended in organic solvents, so they have been considered amphiphobic.[25] As a result, they tend to be displaced from the bulk of either phase and become adsorbed at the water/oil interface.[26] At the same time, metal oxide nanoparticles, such as SiO_2, have been found to be effective in stabilizing Pickering emulsions. Since oxide particles are inherently hydrophilic, the interfacial contact angle bends the interface concave towards the oil, producing oil-in-water emulsions.[27–31]

In the case of recently developed nanohybrids, we demonstrated that the hydrophilic/lipophilic balance (HLB) can be modified by tailoring the composition and structure of the CNT–metal oxide nanoparticle. This fine control of the HLB allowed us to systematically change the type of emulsion, the droplet size, and the volume fraction of the emulsion in the water/oil mixture.[22]

Additionally, by anchoring metal particles on the surface of these nanohybrids, as well as by using nanohybrids composed of CNTs fused to basic metal oxides (e.g., MgO), metal-catalyzed, as well as base-catalyzed, reactions were performed at the water/oil interface in emulsion systems.[21] These reactions have potential applications in many fields of the chemical and fuel industry, such as the upgrading of bio-oils. For instance, we used Pd particles supported on SWCNT–SiO_2 as a catalyst in the hydrodeoxygenation of heavy oxygenated molecules (vanillin) and hydrogenation/etherification of aldehydes (glutaraldehyde and octanal), whereas SWCNT–MgO acted as a basic catalyst for cross-condensation reactions of ketones and aldehydes.[21]

In conventional phase-transfer catalysis,[32–34] a liquid surfactant is typically used to enhance the transfer of molecules between phases, but this emulsion stabilizer cannot be recovered

[a] Dr. M. P. Ruiz, J. Faria, Dr. M. Shen, S. Drexler, T. Prasomsri, Prof. D. E. Resasco
School of Chemical, Biological and Materials Engineering and Center of Interfacial Reaction Engineering, University of Oklahoma
Norman, Oklahoma 73019 (USA)
Fax: (+1) 405-325-5813
E-mail: resasco@ou.edu

after the reaction. In contrast, with the utilization of solid CNT–metal oxide nanohybrid particles the valuable emulsifier/catalyst can be readily recovered by filtration. Similar studies have been performed using solid catalysts at the interface of liquid biphasic systems; however, these studies did not include the formation of emulsions.[35] Several major advantages of using emulsions with the catalyst at the interface are immediately apparent. For example: 1) an enhancement in the rate of mass transfer between phases due to the generation of a higher interfacial area; 2) the possibility of maximizing the selective conversion of molecules present in each of the phases (a concept that we have termed phase-selectivity); 3) the direct partitioning and separation of molecules (phase-migration), simply based on differences in relative solubilities, which leads to a substantial simplification of the purification stage.

Phase-selective catalysis is a desirable approach for any chemical reaction conducted in a biphasic system. Differences in solubility between reactants and a valuable intermediate would facilitate the removal of the intermediate product from the initial phase, while the reactant continues reacting. An example of such a process is the hydrodeoxygenation of heavy oxygenated molecules, typically found in the pyrolysis oil derived from the lignin fraction, which are partitioned in both phases. In a phase-selective process the catalyst that hydrodeoxygenates the water-soluble reactant is present in the aqueous phase. After reaction, the deoxygenated intermediate migrates to the oil phase, in which it could be alkylated by short olefins if an appropriate acid catalyst is present in this phase. As the reactants are consumed in the water phase, more reactant could migrate into this phase and continue reacting.

We previously demonstrated both aqueous and organic phase-selective catalysis.[21,36] Very high selectivity of the reaction on the catalyst facing the aqueous phase was accomplished by taking advantage of the very low density of defects present on the SWCNT walls fused to silica.[21] That is, after the impregnation and calcination of the transition metal on the nanohybrids, the metal particles were preferentially anchored onto the oxide support, leaving the surface of the pristine SWCNTs essentially free of metal due to a much stronger metal–support interaction with the oxide than with the low-defect-density nanotubes. Conversely, we developed oil-phase-selective catalysis by preparing Janus silica particles in which the metal clusters were selectively deposited on the hydrophobic side of the particles.[36]

Herein, we report a study of different carbon structures to be incorporated as the hydrophobic side of the nanohybrids. They include SWCNTs, MWCNTs, and micrographitic platelets (known as "bucky-onions" or "onion-like" carbon).[37] The characteristics of the different emulsions stabilized by these carbon structures, their ability to selectively anchor metal clusters, and the resulting catalytic performance (conversion and phase selectivity) have been compared.

Several reactions of importance in the area of energy production have been used to illustrate this comparison. The first is the hydrogenation of polyaromatics (phenanthrene), which may have an impact in the field of underground (in situ) upgrading of heavy oils by injection of water and nanohybrids into the oil reservoir. The second reaction illustrates the concept of phase-selective catalysis in the organic phase during the simultaneous hydrogenation of glutaraldehyde (water-soluble) and benzaldehyde (oil-soluble) by using physical mixtures of amphiphilic nanohybrids (SWCNT–SiO_2) and pure hydrophobic SWCNTs loaded with Pd clusters. Selective reactions in biphasic systems may have a significant impact in the upgrading of biomass-derived fuels and other chemicals from renewables. The third reaction is the aerobic oxidation of tetralin using Cu catalysts supported on MWCNT–Al_2O_3, demonstrating that the generation of an emulsion improves the catalytic performance compared to the single-phase system. This reaction may have importance in the underground oxidation of aromatics for enhanced oil recovery.

Results and Discussion

Characterization of carbon nanotube/metal oxide hybrids

Carbon structure characterization

The core of this study is the comparison of a series of nanohybrids with different carbon structures. The nanohybrids chosen for this comparison include SWCNT–SiO_2, "onion-like" carbon–SiO_2, MWCNT–Al_2O_3, and nitric acid-oxidized MWCNT–Al_2O_3 (Figure 1). High-resolution TEM (HRTEM) images of the catalysts

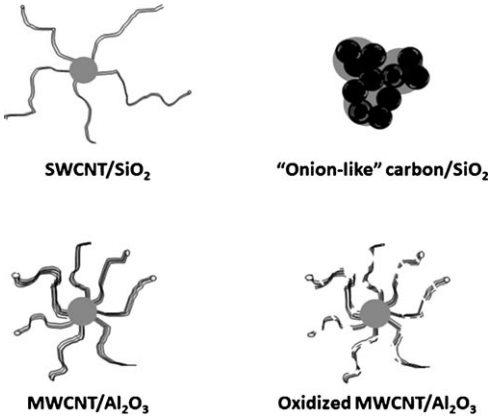

Figure 1. Structures of the nanohybrids.

prepared using these nanohybrids loaded with Pd clusters illustrate the different morphologies of the nanohybrids (Figure 2). The carbon content is also quite different among the samples; the carbon content of SWCNT–SiO_2 is around 7%, that for "onion-like" carbon–SiO_2 is 17%, and for MWCNT–Al_2O_3 it is around 30%. It is worth noting that for "onion-like" carbon–SiO_2 the SiO_2 surface is not totally covered by carbon; X-ray photoelectron spectroscopy (XPS) showed a Si/C ratio (atomic surface concentration) of 2.9. This partial coverage is what imparts the amphiphilic character to the nanohybrid.

Raman spectroscopy has been used to characterize the carbon structure on the various nanohybrids. This technique has been widely employed to evaluate the purity and quality

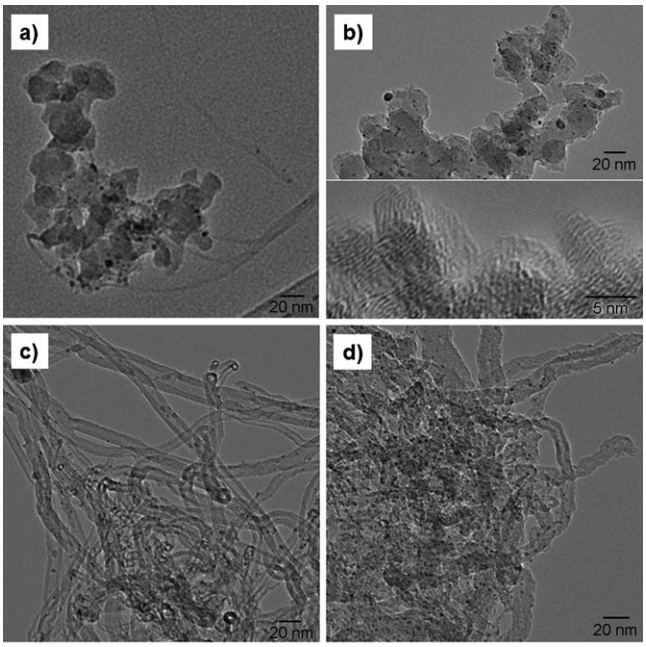

Figure 2. HRTEM images of the catalysts composed of 5 wt% Pd supported on different nanohybrids: a) SWCNT–SiO_2; b) "onion-like" carbon–SiO_2 (top; Pd on the nanohybrid; bottom; closer view of the "onion-like" carbon in the nanohybrid); c) MWCNT–Al_2O_3; d) oxidized MWCNT–Al_2O_3. The average size of the Pd clusters are: a) 4.9, b) 4.6, c) 3.0, and d) 2.1 nm, for the corresponding nanohybrids.

of CNT products.[38–40] The relative density of defects in different CNT samples has been typically evaluated in terms of two characteristic bands; the G band, which appears at about 1590 cm^{-1}, is ascribed to sp^2 ordered carbon atoms and the D band, which appears at about 1350 cm^{-1}, is commonly ascribed to sp^3 carbon atoms associated with defects.[41–43] Figure 3 shows the normalized Raman spectra for the different nanohybrids, together with the calculated D/G intensity ratios. SWCNT–SiO_2 has the smallest D/G ratio (0.09), consistent with a low density of defects. "Onion-like" carbon–SiO_2 has an intermediate value (1.1), whereas the most defective carbon structures are MWCNT–Al_2O_3 and oxidized MWCNT–Al_2O_3 (D/G ratios of 2.3 and 2.7, respectively). A small, but noticeable change in the intensity of the D band is observed upon oxidation.

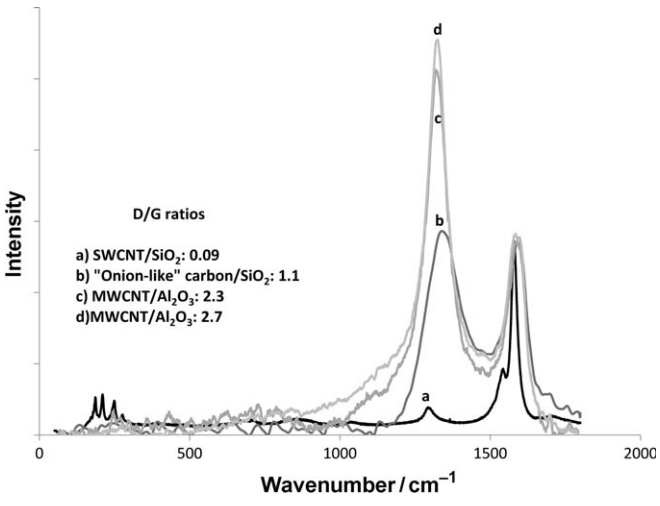

Figure 3. Raman spectra of the nanohybrids: a) SWCNT–SiO_2, b) "onion-like" carbon–SiO_2, c) MWCNT–Al_2O_3, and d) oxidized MWCNT–Al_2O_3.

The effect of nitric acid oxidation on MWCNT–Al_2O_3 was evaluated by using XPS. Figure 4 shows the C 1s spectra for MWCNT–Al_2O_3, before and after oxidation. Again, a slight but noticeable difference can be seen in the region of 286 eV,

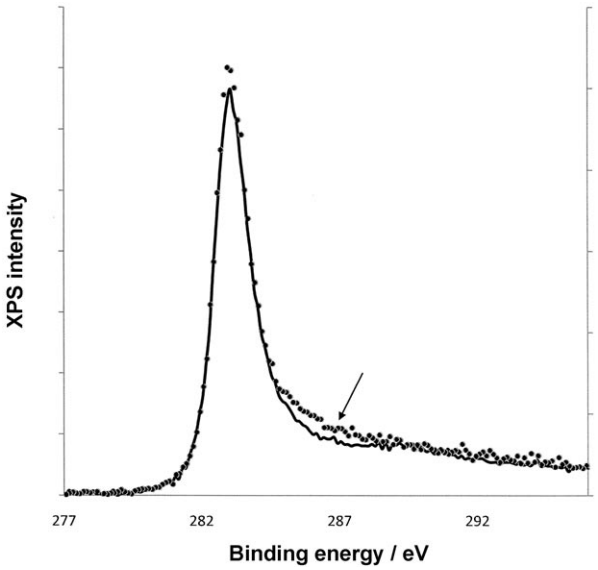

Figure 4. XPS spectra (C 1s) of MWCNT–Al_2O_3 and oxidized MWCNT–Al_2O_3. —— MWNT/Al_2O_3; ● oxidized MWNT/Al_2O_3. The arrow shows the region of functionalized carbon where the most significant difference is observed.

which can be ascribed to the formation of carboxylic groups upon the nitric acid oxidation treatment. To quantify these changes, a conventional acid–base titration method was used to determine the concentration of acid sites on these nanohybrids. The results showed concentrations of 3.3 and 6.5 mmol acid sites per gram of nanohybrids on MWCNT–Al_2O_3 and oxidized MWCNT–Al_2O_3, respectively, in accordance with the results obtained by XPS.

DFT calculations

To understand the ability of wall defects in stabilizing Pd nanoclusters, density functional theory (DFT) calculations were conducted to compare the strength of the metal–carbon interaction on an oxidized defect site to that on a pristine carbon wall. In a recent study,[44] we used ONIOM (DFT:MM) calculations to show that the binding energy of Pd clusters was significantly enhanced when the SWCNT surface was oxygen functionalized, compared to that on a pristine SWCNT surface. The electronic interaction of Pd atoms with oxygen at the defect sites resulted in stronger bonding (4.6 eV in comparison with 2.6 eV).

In this study, the adsorption of Pd nanoclusters on MWCNTs was also theoretically investigated. Three layers of graphene sheets were used as a representative of the MWCNT surface (Figure 5). The interlayer distance and a typical C–C bond

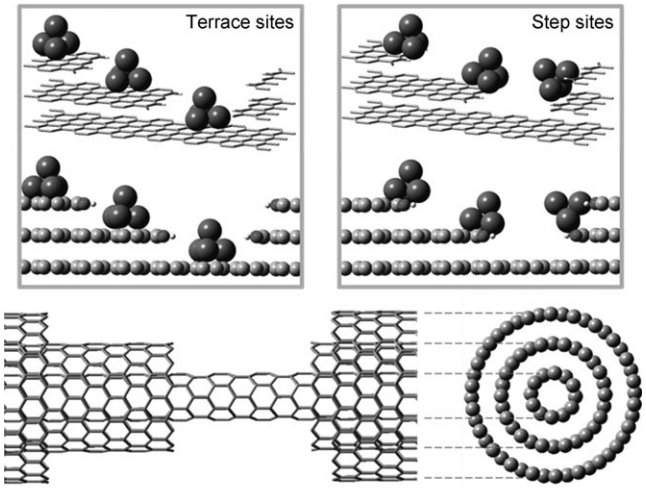

Figure 5. Models for Pd cluster adsorption on terrace sites (left) and step sites (right) of MWCNTs.

length are approximately 3.4 Å and ca.1.41 Å, respectively.[45] Each C dangling bond at the edges of the step sites was terminated with a carboxyl functional group. Adsorption energies of Pd nanoclusters on terrace sites and step sites were examined to elucidate the role of defects containing the functional group.

Spin-polarized periodic DFT calculations were performed using the Vienna ab initio simulation package (VASP),[46–50] in which the Kohn–Sham equations are solved by self-consistent algorithms. The dimensions of the unit cells are: $a=9.769$ Å, $b=29.160$ Å, $c=30.00$ Å, and $\alpha=\beta=\gamma=90^{\circ}$. A cutoff energy of 300 eV was used. Brillouin zone sampling was restricted to the Γ point. Pd nanoclusters were freely optimized and a quasi-Newton forces-minimization algorithm was employed for the forces-minimization algorithm. Convergence was assumed to be achieved when forces were below 0.05 eV Å^{-1}. The adsorption energy, E_{ads}, is given by Equation (1):

$$E_{ads} = E_{Pd/MWCNT} - E_{MWCNT} - E_{Pd} \quad (1)$$

in which, $E_{Pd/MWCNT}$ is the total energy of the MWCNTs with Pd clusters, E_{MWCNT} is the energy of the MWCNTs, and E_{Pd} is the energy of the Pd clusters in gas phase.

Based on the calculation, the binding energy on the step sites is 1.36 eV higher than that on the terrace sites of MWCNTs. This demonstrates the preferential adsorption of Pd nanoclusters on oxidized defects of MWCNTs, which is consistent with our previous study on SWCNTs[44] and the experimental results of this study.

Nanohybrids as emulsion stabilizers

Emulsion structures

The ability of the different nanohybrids (SWCNT–SiO_2, "onion-like" carbon–SiO_2, MWCNT–Al_2O_3, and oxidized MWCNT–Al_2O_3) to stabilize water/decalin emulsions was compared. Illustrative microscope images of the different emulsions are shown in Figure 6. There are clear differences in the emulsion characteristics upon changing the type of nanohybrids. Figure 7 shows

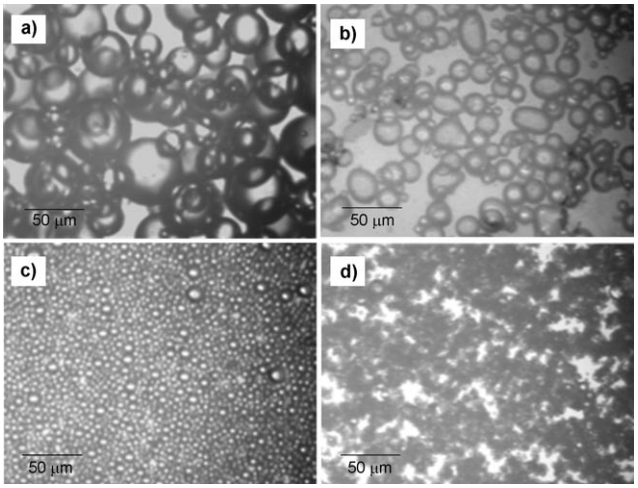

Figure 6. Microscope images of the water/decalin emulsions stabilized with a concentration of 1 wt% of nanohybrids: a) SWCNT–SiO_2; b) "onion-like" carbon–SiO_2; c) MWCNT–Al_2O_3; d) oxidized MWCNT–Al_2O_3.

the changes in emulsion volume fraction and the average droplet size obtained with the different nanohybrids. The effect of changing the concentration of nanohybrids was also investigated, as we have shown previously that the particle concentration strongly affects both the emulsion volume stabilized and the droplet size.[22,51,52] In general, for all of the nanohybrids, an increase in particle concentration led to an increase in the fraction of emulsion stabilized and a decrease in the size of the emulsion droplets. The higher viscosity of the medium when increasing the particle concentration may play a role in stabilizing smaller droplets.[22] Comparing the behavior of the different nanohybrids, it can be concluded that the most effective nanohybrid in stabilizing interfacial area in emulsions is oxidized MWCNT–Al_2O_3, since for a given concentration it gave the highest values of emulsion fractions (up to 0.85) with the smallest droplet sizes (less than 2 μm). Accordingly, the effectiveness in stabilizing emulsions follows this sequence: oxidized MWCNT–Al_2O_3 > MWCNT–Al_2O_3 > "onion-like" carbon–SiO_2 > SWCNT–SiO_2.

Depending on the HLB in the composition of the nanohybrids, it is possible to stabilize either water-in-oil or oil-in-water emulsions. We have previously shown that when the particles were more hydrophilic, the wettability of the particles in water was enhanced, making the interface bend concave towards the oil, producing oil-in-water emulsions. In contrast, more hydrophobic particles tended to form water-in-oil emulsions.[53]

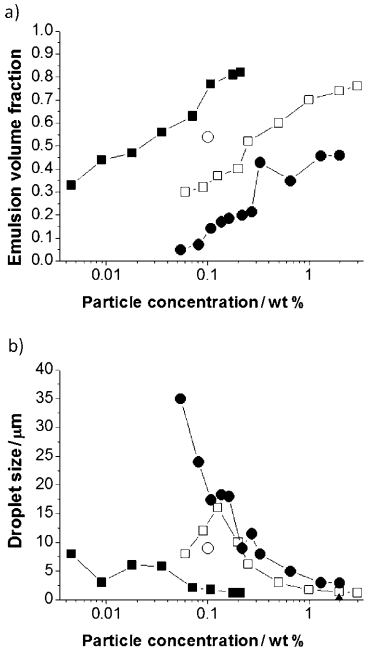

Figure 7. a) Emulsion volume fraction and b) droplet size versus particle concentration for the water/decalin emulsions prepared with the nanohybrids. ● SWCNT–SiO_2;[22] □ "onion-like" carbon–SiO_2; ○ MWCNT–Al_2O_3; ■ oxidized MWCNT–Al_2O_3.

Under the conditions studied here, the more hydrophobic SWCNT–SiO_2 and MWCNT–Al_2O_3 produced water-in-oil emulsions. In contrast, "onion-like" carbon–SiO_2 and oxidized MWCNT–Al_2O_3 stabilized oil-in-water emulsions owing to their higher hydrophilic character, caused by their higher density of oxidized defects.

Emulsion interface characterization

The interface of the emulsion stabilized by the nanohybrids was characterized by taking TEM images of a freeze-fractured surface replica of a water-in-decalin droplet stabilized by SWCNT–SiO_2 (Figure 8). The TEM images clearly show how the CNTs are generally oriented towards the oil phase, whereas the silica particles remain near the water phase.

Further characterization of the interface was performed using XPS. A catalyst composed of Pd anchored on SWCNT–SiO_2 was analyzed before and after being used to stabilize an emulsion. In the first case, the catalyst was analyzed directly after its preparation, whereas in the second case it was first used to stabilize a water-in-oil (decalin) emulsion, and then vacuum-dried and the remaining catalyst particles were analyzed. Figure 9 illustrates the expected morphology of the catalyst aggregates in both cases. When the catalyst was used to stabilize the emulsion, we expected that the CNTs on the nanohybrids particles preferentially orient towards the oil phase (Figure 8), with more metal particles facing the surface than in the absence of the interface. This is in accordance with the results obtained by XPS (Table 1), that show a higher intensity ratio of C/Si and Pd/Si when the catalyst has been used to stabilize the emulsion (20.8 and 15.4×10^{-2}, respectively), in comparison with the initial catalyst (6.9 and 5.2×10^{-2}, respectively).

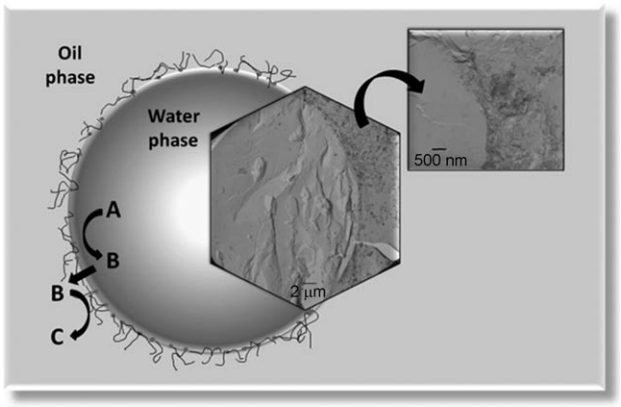

Figure 8. TEM images of the interface in a water-in-oil emulsion droplet stabilized by SWCNT–SiO_2, together with a general reaction scheme.

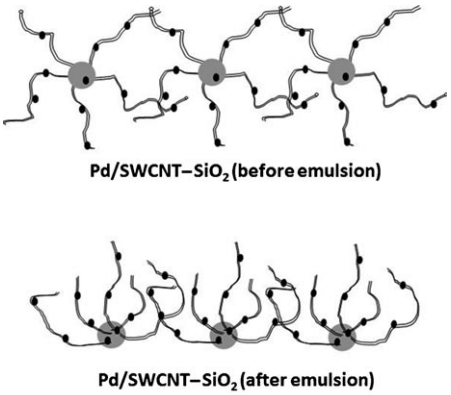

Figure 9. Pd/SWCNT–SiO_2 structure before and after emulsion.

Table 1. C/Si and Pd/Si intensity ratios obtained from the XPS analysis of dried Pd/SWCNT–SiO_2 and Pd/SWCNT–SiO_2 in emulsion.

	C/Si	Pd/Si
Pd/SWCNT–SiO_2 (dried)	6.9	5.2×10^{-2}
Pd/SWCNT–SiO_2 (in emulsion)	20.8	15.4×10^{-2}

Reactions at the water/oil interface in emulsion systems

The use of nanohybrids as supports of metal particles to perform reactions at the water/oil interface has allowed us to take advantage of an enhanced interfacial area, an easier product separation by differences in solubility, as well as a method for simple catalyst recovery. The process of interfacial catalysis followed by phase-transfer is summarized in Figure 8, together with a generic reaction scheme. In the generic example, we show the conversion of a water-soluble compound **A** that when it reaches the interface is catalytically converted into **B**, which has a lower solubility in water. Compound **B** would partition between the two phases, and could react further in the

oil phase to produce **C**. The differences in solubility of the products and reactant facilitate their separation.

The three reaction examples studied in this work are the hydrogenation of phenanthrene, hydrogenation of glutaraldehyde and benzaldehyde, and oxidation of tetralin.

Hydrogenation of phenanthrene

The first reaction system investigated was the hydrogenation of phenanthrene, which is a solid under atmospheric conditions, but is highly soluble in organic compounds. Therefore, in this system, the phenanthrene was present only in the oil phase dissolved in decalin. Not all the solubility values of a given compound in a given medium are readily available. Therefore, a parameter that can help to predict the solubility behavior of a given molecule in water/oil systems is the octanol–water partition coefficient log *P*. This value has been widely used in rational drug design and other quantitative structure–activity relationship (QSAR) property prediction studies as a measure of the hydrophobicity/hydrophilicity ratio of a given molecule. High log *P* values are indicative of a higher affinity of the molecule for the organic phase, and vice versa. The log *P* values can be calculated by using an interactive log *P* calculator (www.molinspiration.com/services/logp.html). For example, the log *P* of phenanthrene is 4.304.

To perform the hydrogenation reactions, catalysts composed of 5 wt% Pd supported on the different types of nanohybrids (SWCNT–SiO_2, "onion-like" carbon–SiO_2, MWCNT–Al_2O_3, and oxidized MWCNT–Al_2O_3) were used. The aim of this study was to compare the performance of different carbon structures as a support for the metal clusters, as well as stabilizers for the emulsion system. Some HRTEM images of the final catalysts are shown in Figure 2. A simple analysis of the Pd cluster size distribution indicates that the resulting Pd dispersion is rather low on SWCNT–SiO_2 and "onion-like" carbon–SiO_2, with an average Pd cluster size of approximately 5 nm, but there is significantly higher dispersion on oxidized MWCNT–Al_2O_3 (Figure 2d), with an average Pd cluster size of less than 1 nm. It appears that the oxidation of MWCNT–Al_2O_3 with nitric acid has created a high number of oxidized defects on the nanotubes, as demonstrated by the Raman and XPS results (Figure 3 and 4), which, according to the DFT calculations, enhance the interaction and favor the dispersion of the Pd clusters.[44] The non-oxidized MWCNT–Al_2O_3 resulted in a Pd cluster dispersion that was not as good as that observed with the oxidized ones, but was still better than those obtained on SWCNT–SiO_2 and "onion-like" carbon–SiO_2 nanohybrids.

As shown in Figure 10, the conversion of phenanthrene increases in the following order: SWCNT–SiO_2 < "onion-like" carbon–SiO_2 < MWCNT–Al_2O_3 < oxidized MWCNT–Al_2O_3. It is clear that, for a given set of reaction conditions, the conversion is influenced by two phenomena, which are different in nature but both improve conversion. One effect is the dispersion of the Pd clusters on the surface of the nanohybrids, which increases with the density of oxidized defects. The second effect is the higher effectiveness of the nanohybrids for the stabilization of the emulsion as the density of defects increases; for example, a shift in the HLB to higher hydrophilicity enhances the total interfacial area created by the nanohybrid. Both effects, a higher interfacial area and a better dispersion of the metal clusters, result in higher conversions (Figure 10).

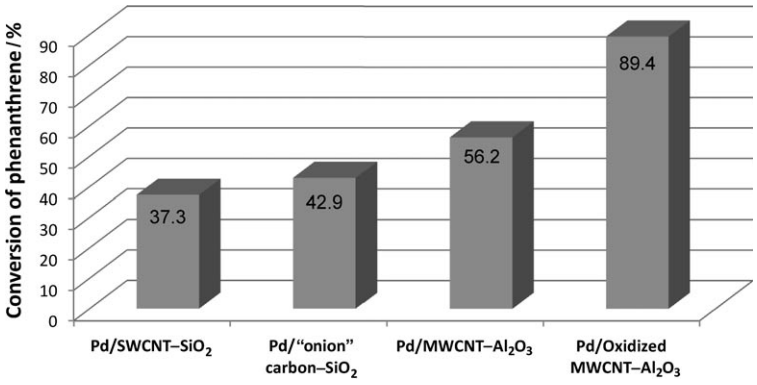

Figure 10. Conversion obtained in the hydrogenation reactions of phenanthrene over catalysts comprising 5 wt% Pd supported on different nanohybrids. Reaction conditions: Semi-batch reactor, catalyst (30 mg), water/decalin (30 mL, 1:1 v/v), $T = 200\,^{\circ}C$, H_2 (6.21 MPa), $t = 24$ h.

The most active catalyst was that supported on acid-oxidized MWCNT–Al_2O_3, which, for the same solid concentration, exhibited the highest fraction of emulsion and the smallest droplet size among the series of different nanohybrids (Figure 7). In addition, the dispersion of Pd clusters on oxidized MWCNT–Al_2O_3 was higher than on other supports, as a result of a stronger metal–support interaction.[54] A final, albeit very important, consideration is the tendency of the carbon nanohydrids to aggregate when placed in the liquid phase. The nitric acid oxidation treatment greatly enhances the repulsion between the MWCNTs, which increases their emulsification efficiency (Figures 6 and 7).

The second most active catalyst was the non-oxidized MWCNT–Al_2O_3, which stabilized a high interfacial area and metal dispersion. The conversion of phenanthrene with this material was relatively high (56%; Figure 10). Whereas the other two nanohybrids SWCNT–SiO_2 and "onion-like" carbon–SiO_2 showed similar Pd dispersion, the emulsion droplet stabilized by the latter was significantly smaller than that stabilized by the former, and led to a slightly higher phenanthrene conversion (43% with "onion-like" carbon–SiO_2 versus 37% with SWCNT–SiO_2).

The reaction pathway for the phenanthrene hydrogenation is shown in Scheme 1. It must be noted that all the products from the hydrogenation of phenanthrene are highly soluble in the organic phase (log $P > 4$). The two main products from the hydrogenation of phenanthrene were 9,10-dihydrophenanthrene and 1,2,3,4-tetrahydrophenanthrene (Table 2). However, when high levels of conversion were reached (83%, in the case of oxidized MWCNT–Al_2O_3), formation of 1,2,3,4,4a,9,10,10a-octahydrophenanthrene and 1,2,3,4,5,6,7,8-octahydrophenanthrene readily occurred. This sequential hydrogenation has pre-

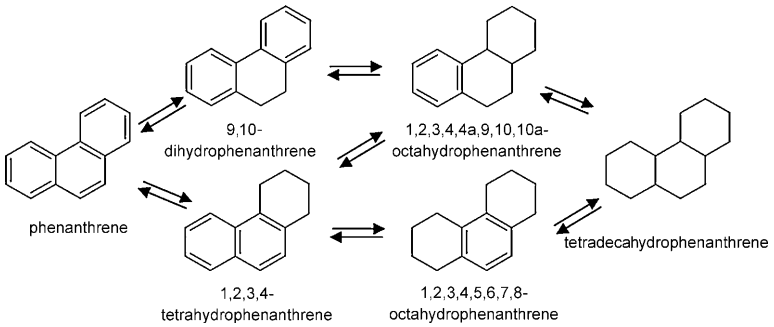

Scheme 1. Phenanthrene hydrogenation mechanism.

Table 2. Product yields (%) obtained in the hydrogenation of phenanthrene with catalysts composed of 5 wt% Pd supported on nanohybrids. Reaction conditions: Semi-batch reactor, catalyst (30 mg), water/decalin (30 mL, 1:1 v/v), $T = 200\,^{\circ}C$, H_2 (6.21 MPa), $t = 24$ h.

	P1[a]	**P2**[b]	**P3**[c]	**P4**[d]	**P5**[e]
Pd/SWCNT–SiO_2	59.6	19.3	6.3	11.2	3.6
Pd/"onion-like" carbon–SiO_2	68.8	16.8	2.5	10.0	2.0
Pd/MWCNT–Al_2O_3	62.5	22.8	5.4	6.9	2.5
Pd/oxidized MWCNT–Al_2O_3	67.2	7.3	8.7	15.6	1.2

[a] **P1** = 9,10-dihydrophenanthrene. [b] **P2** = 1,2,3,4-tetrahydrophenanthrene. [c] **P3** = 1,2,3,4,4a,9,10,10a-octahydrophenanthrene. [d] **P4** = 1,2,3,4,5,6,7,8-octahydrophenanthrene. [e] **P5** = tetradecahydrophenanthrene.

viously been observed and is an indication of the important role of the adsorption-site competition, in which the more aromatic compound always dominates on the surface. That is, conversion of the one-ring aromatic species does not happen until most of the 3- and 2-ring compounds have been hydrogenated.[55]

Simultaneous hydrogenation of glutaraldehyde and benzaldehyde

The simultaneous hydrogenation of glutaraldehyde (water-soluble) and benzaldehyde (oil-soluble) has been studied in an emulsion system. Two different catalysts have been used as stabilizers/catalysts in these reactions to test the concept of phase-selectivity. One of the catalysts was 5 wt% Pd/SWCNT–SiO_2 and the other was a physical mixture of metal-free nanohybrids (SWCNT–SiO_2) and silica-free 10 wt% Pd/SWCNT (1:1 w/w). In this mixture, the hydrophobic Pd/SWCNT remains in the oil side, but the strong tube–tube interaction keeps them at the water/oil interface, connected to the amphiphilic nanohybrids. Therefore, this system results in efficiently dispersed Pd catalyst, albeit located only in the organic phase. On the contrary, in the Pd/SWCNT–SiO_2, the metal is deposited over the entire support, that is, on the hydrophobic as well as hydrophilic sides. Therefore, this catalyst should be able to catalyze reactions in both phases of the emulsion. However, we cannot expect that the amount of Pd on the SWCNTs will be as high as on the silica, since, during the incipient wetness impregnation, the metal precursors tends to deposit more on the oxide support than on the pristine (unfunctionalized) SWCNTs.

The conversions of glutaraldehyde and benzaldehyde obtained with the two different catalysts after 3 h of reaction at 100 °C and 1.38 MPa of H_2, are shown in Figure 11. First, it is noted that the conversion of the organic-soluble benzaldehyde is

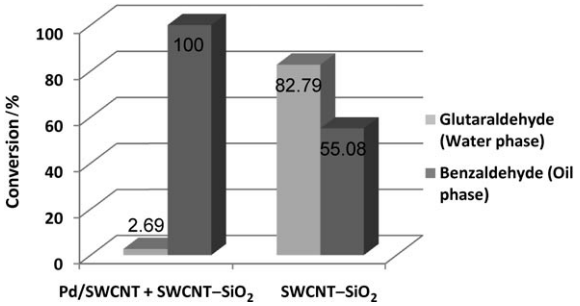

Figure 11. Conversion of glutaraldehyde and benzaldehyde obtained in the hydrogenation reactions over two different catalysts; the former composed of a mixture of SWCNT–SiO_2 nanohybrids and Pd deposited on purified SWCNTs (Pd present only in the oil phase), and the latter composed of Pd deposited on SWCNT–SiO_2 nanohybrids (Pd present in both phases). Reaction conditions: Semi-batch reactor, catalyst (30 mg), water/decalin (30 mL, 1:1 v/v), $T = 100\,^{\circ}C$, H_2 (1.38 MPa), $t = 3$ h.

100% when Pd is only in the oil phase and 55% when Pd is present in both phases. As mentioned above, a larger fraction of Pd deposits on the oxide than on the SWCNTs (Figure 2a), which explains the lower conversion obtained when Pd is distributed among the two parts of the nanohybrid.

The behavior observed with the water-soluble glutaraldehyde under the same conditions was, as expected, opposite to that of benzaldehyde. That is, the conversion was 83% when the catalyst with Pd deposited on the two sides of the nanohybrids was employed, but less than 3% when the catalyst with Pd only deposited on the hydrophobic side was present. The phase-selective catalysis in the organic phase is clearly demonstrated in these experiments. In our previous study, we demonstrated the water phase-selectivity using nanohybrids[21] and Janus silica particles.[36]

The final composition of both phases after these reactions is summarized in Table 3. The reaction network and corresponding products for the hydrogenation of glutaraldehyde catalyzed by Pd can be found in our previous report.[36] The hydrogenation of benzaldehyde only produced benzyl alcohol (Table 3). It is worth noting that, whereas benzaldehyde only appeared in the organic phase, benzyl alcohol was partitioned between the two phases (log *P* values were 1.740 and 1.270, respectively).

Different products were obtained from the hydrogenation of glutaraldehyde (Table 3). When Pd was present on the hydro-

Table 3. Product composition (%) obtained in the hydrogenation reactions over two different catalysts; the former composed of a mixture of SWCNT–SiO_2 nanohybrids and Pd deposited on purified SWCNT (Pd present only in the oil phase), and the latter composed of Pd deposited on SWCNT–SiO_2 nanohybrids (Pd present in both phases). Reaction conditions: Semi-batch reactor, catalyst (30 mg), water/decalin (30 mL, 1:1), $T=100\,^{\circ}C$, H_2 (1.38 MPa), $t=3$ h.

		Pd/SWCNT+SWCNT–SiO_2	Pd/SWCNT–SiO_2
water phase	glutaraldehyde	69.6	11.8
	δ-valerolactol	1.9	20.6
	1,5-pentanediol	0.0	35.6
	5-(tetrahydro-2*H*-pyran-2-yloxy)pentan-1-ol	0.0	0.1
	benzyl alcohol	28.5	31.9
oil phase	benzaldehyde	0.0	70.0
	benzyl alcohol	100.0	29.1
	5-(tetrahydro-2*H*-pyran-2-yloxy)pentan-1-ol	0.0	0.9

philic side (high conversion of glutaraldehyde), the cyclic hemiacetal δ-valerolactol was observed as the main product, together with the fully hydrogenated 1,5-pentanediol. Another product, formed in lower yields when Pd was present in the hydrophilic side, was the ether 5-(tetrahydro-2*H*-pyran-2-yloxy)pentan-1-ol. Our group recently showed that alcohols and aldehydes react on Pd to form ethers.[56] In this case, it seems that δ-valerolactol and 5-hydroxypentanal in the aqueous phase readily form the ether, which tends to partition between the organic and aqueous phases (log $P=1.578$).[36] In contrast, both δ-valerolactol and 1,5-pentanediol remained in the aqueous phase due to their high solubility in water (log P values were 0.547 and 0.095, respectively).

Partial oxidation of tetralin

The third reaction used as an example for the interfacial catalysis concept was the partial oxidation of tetralin in both emulsion and single organic phase (tetralin) to evaluate the effect of the formation of the emulsion on conversion and selectivity. The catalyst used for this reaction was 10 wt% Cu/MWCNT–Al_2O_3. The two main products obtained upon the oxidation of tetralin (1,2,3,4-tetrahydronaphtalene) were α-tetralone (3,4-dihydronaphtalen-1(2*H*)-one) and α-tetralol (1,2,3,4-tetrahydronaphtalen-1-ol). Under the reaction conditions investigated, a small fraction of α-tetralol further decomposed to form 1,2-dihydronaphtalene with yields less than 1%. Figure 12 compares the different levels of conversion obtained after reaction times of 3 and 6 h. It is clear that higher tetralin conversion is obtained in the emulsion than in the single phase (0.1 versus 26%, respectively, after 3 h, and 14 versus 42%, respectively, after 6 h). This difference could be attributed to the higher level of aggregation of the catalyst in the single-phase system and to the decreased oxygen concentration in the medium, due to the lower solubility of oxygen in tetralin compared to that in water. In addition, in the emulsion system, the enhanced water/oil emulsion interfacial area improves mass transfer of molecules between the phases.

The widely accepted pathway of this reaction is depicted in Scheme 2.[57,58] A tetralin hydroperoxide species is believed to be a crucial intermediate. This hydroperoxide appears to be involved even in the thermal oxidation reaction. However, whereas in the thermal reaction the distribution of products is about equimolar in α-tetralone and α-tetralol,[59] in the presence of a catalyst is greatly varied.[57] For example, we see here that in the case of Cu, the tetralone/tetralol ratio is much greater than one. It is possible that the presence of an emulsion may have an effect on the concentration of the hydroperoxide intermediate. For example, a long induction period is clearly noticeable when the reaction is conducted in the single phase, but this induction period disappears when it is conducted in the emulsion system. It is possible that a higher concentration of the crucial hydroperoxide intermediate is built up much more rapidly.

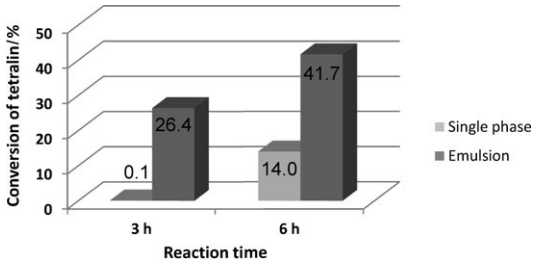

Figure 12. Conversion of tetralin obtained in oxidation reactions performed in single phase and in emulsion, both at two different times ($t=3$ and 6 h). Reaction conditions: Semi-batch reactor, catalyst in tetralin (2 mg mL^{-1}), $T=80\,^{\circ}C$, air (1.38 MPa).

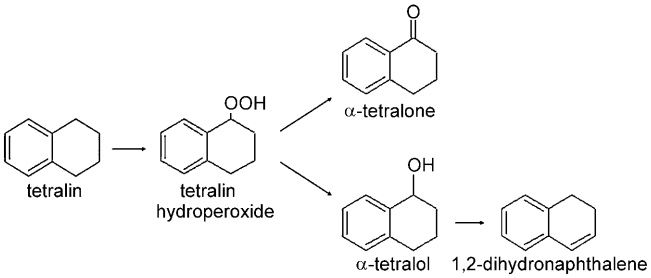

Scheme 2. Tetralin oxidation mechanism.

Conclusion

A series of different amphiphilic nanohybrids based on SWCNTs and MWCNTs (hydrophobic side) fused to different metal oxide particles (hydrophilic side) have been investigated as stabilizers of water/oil emulsions, as well as supports for

metal clusters that catalyze reactions at the water/oil interface in emulsion systems. The catalytic performances of the different nanohybrids (SWCNT–SiO_2, "onion-like" carbon–SiO_2, and MWCNT–Al_2O_3) doped with palladium were compared in three different reactions: 1) Hydrogenation of phenanthrene; 2) hydrogenation of glutaraldehyde and benzaldehyde; 3) partial oxidation of tetralin. The nanohybrids have a dual purpose, as stabilizers of emulsion and as supports for anchoring catalytic species. They present the following advantages: Higher interfacial area, enhanced mass transfer of compounds between the two phases, effective product separation by differences in solubility, and most importantly, recoverability and recyclability after reaction.

The main conclusions of the study can be summarized as follows:

1) The comparison of the performance of the Pd-loaded nanohybrids with different carbon morphology in the hydrogenation of phenanthrene demonstrated that the observed activity is directly related to the nature of the emulsion that is stabilized and the dispersion of Pd clusters. Both characteristics can be controlled by varying the nanohybrid structure. It is clear that the nanohybrids found to be most effective for stabilizing emulsions and dispersing metal clusters are also the most active catalysts.

2) The concept of phase-selective catalysis occurring in the emulsion system with a two-faced catalyst has been demonstrated in the simultaneous hydrogenation of glutaraldehyde (aqueous) and benzaldehyde (organic), by keeping the Pd clusters only facing the organic phase and, thus, results in selective conversion only on that side.

3) The study of the partial oxidation of tetralin, using Cu deposited on MWCNT–Al_2O_3 as a catalyst, showed a higher conversion in the emulsion system than in the single-phase (oil) system and the reduction of the induction period due to a more effective confinement of the hydroperoxide intermediate in the emulsion system.

Experimental Section

Materials

The nanohybrids SWCNT–SiO_2, MWCNT–Al_2O_3, and purified SWCNTs were provided by SouthWest NanoTechnologies. The SWCNT–SiO_2 preparation is based on the CoMoCAT synthesis process developed by our group and is capable of consistently producing SWCNTs of high quality.[60–62]

Oxidized MWCNT–Al_2O_3 nanohybrids were prepared by treating MWCNT–Al_2O_3 with nitric acid as follows. MWCNT–Al_2O_3 (1 g) was treated with HNO_3 (16 M, 50 mL) and stirred for 3 h at 110 °C. The final product was filtered and washed with deionized water until neutral pH was reached, and then dried overnight at 100 °C.

For the preparation of "onion-like" carbon–SiO_2, silica Aerosil 200 (from Evonik–Degussa) was impregnated with an aqueous solution of $Co(NO_3)_2{\cdot}6H_2O$ and $(NH_4)_6Mo_7O_{24}{\cdot}4H_2O$ (provided by Sigma Aldrich), reaching a final metal loading of 2 wt%, with a Co/Mo molar ratio of 1:3. The powder was then calcined in air following this sequence: 1 h at 100 °C, 1 h at 200 °C, 1 h at 300 °C, and 2 h at 500 °C. After cooling to room temperature, the catalyst (1 g) was placed in a reactor where it was first reduced under H_2 (300 mL min^{-1} flow rate) at 500 °C for 30 min, then heated up to 700 °C in He (300 sccm), and finally exposed at that temperature to C_2H_4 (400 sccm) in He (1:3 molar ratio) for 20 min. The final product ("onion-like" carbon–SiO_2, as shown by TEM) was then allowed to cool to room temperature in He.

Characterization techniques

The nanohybrids were characterized by HRTEM, Raman spectroscopy, and XPS. The HRTEM images were obtained on a JEOL JEM-2100 scanning transmission electron microscope system. The Raman spectra were acquired on a Jovin Yvon-Horiba Lab Ram equipped with a charge-coupled detector and a He–Ne laser ($\lambda =$ 632 nm) as excitation source. The XPS spectra were recorded on a Physical Electronics PHI 5800 ESCA system, equipped with an Al KR X-ray anode operated at 350 W and 15 kV. The base pressure of the main chamber was kept at about 1.33 μPa.

The acid–base titration method used to determine the concentration of acid sites on both MWCNT–Al_2O_3 and oxidized MWCNT–Al_2O_3, was previously described by Hu et al.[63] It consisted of three main steps: First, nanohybrids (100 mg) were stirred in NaOH (0.05 N, 50 mL) for 48 h in an inert atmosphere; then, the nanohybrids were filtered and washed with deionized water, and the filtrate together with the washing water were mixed with HCl (0.05 N, 50 mL). Finally, the excess of acid was titrated with a solution of NaOH (0.05 N) until neutral pH was reached. From the volume of NaOH used in the last step and the initial volumes of NaOH and HCl employed, it was possible to calculate the concentration of acid sites in the nanohybrids.

Preparation of emulsions using different nanohybrids

To prepare the water/oil emulsions for characterization of the properties (type of emulsion and droplet size) with the different nanohybrids, deionised water and decalin were used as the aqueous and organic phases, respectively. The nanohybrids were first dispersed in the water phase by sonication with a Horn sonicator (Fisher Scientific 600 W, 20 kHz) at 25% of amplitude for 30 min. Then, decalin was added (water/decalin, 1:1) and the final mixture sonicated for 1 h. The amount of nanohybrids was varied as described above. A green water-soluble dye (fluorescent Na salt) and a red oil-soluble dye (Sudan III) were added to the respective phases to identify the corresponding emulsion fractions.

Hydrogenation of phenanthrene

The hydrogenation reactions were carried out in a semi-batch Parr 4843 reactor of 50 mL. A detailed description of the reaction system can be found in a previous publication.[21,36] In each experiment, deionised water (15 mL) and decalin (15 mL) were placed into the reactor vessel with the catalyst (30 mg). The mixture was sonicated for 15 min using a Horn sonicator to produce the emulsion in situ. Then, the reactor vessel was assembled in the reaction system.

After purging with N_2, a flow of pure H_2 (110 sccm) was passed through the reactor for 3 h at 100 °C and 1.38 MPa. Then, the temperature and pressure were adjusted to 200 °C and 6.21 MPa, re-

spectively, before the reactant (a solution of phenanthrene (0.03 M) in decalin) was injected. During the entire reaction period the flow of gases was kept constant at 110 sccm, while the liquid mixture was kept in the reactor with the use of a condenser that returns the vapors back to the vessel and minimize liquid loss. After 24 h, the reaction was stopped by turning off the heater and switching H_2 to N_2. Once the reactor reached RT, it was taken apart and the contents filtered, which allowed the full recovery of the catalysts and the breaking of the emulsion into two clear liquid phases (aqueous and organic). The composition of each phase was analyzed independently by GC-MS and GC with a flame-ionization detector (FID).

To prepare the 5 wt% Pd catalysts on the various nanohybrid supports (SWCNT–SiO_2, "onion-like" carbon–SiO_2, MWCNT–Al_2O_3, and oxidized MWCNT–Al_2O_3) the incipient wetness impregnation method was followed, using an aqueous solution of the metal precursor [$Pd(NO_3)_2{\cdot}x\,H_2O$ (provided by Sigma Aldrich)]. After impregnation, the catalysts were dried overnight at 100 °C and then calcined in He at 300 °C for 2 h.

Hydrogenation of glutaraldehyde and benzaldehyde

The hydrogenations of glutaraldehyde and benzaldehyde were carried out in the same system as the hydrogenation of phenanthrene. The reduction of the catalysts was performed under the same conditions. However, the reaction conditions in this case were 100 °C and 1.38 MPa H_2, and 3 h of reaction time. The initial concentration of reactants was glutaraldehyde (0.3 M) in the water phase and benzaldehyde (0.3 M) in the oil phase (decalin).

In this case, the performance of a catalyst composed of 5 wt% Pd on SWCNT–SiO_2 was compared with another a physical mixture (wt ratio 1:1) of metal-free SWCNT–SiO_2 and pure SWCNTs doped with 10 wt% Pd. In the former, the Pd was deposited on the entire surface of the nanohybrids (on both the SWCNTs and silica) whereas in the latter the Pd particles were only deposited on the SWCNTs. To deposit Pd, both SWCNT–SiO_2 and purified SWCNTs were impregnated with the same procedure as described above for the catalysts used in the hydrogenation of phenanthrene. The drying and calcination conditions were also the same.

Oxidation of tetralin

The partial oxidation of tetralin was performed in a 4590 Parr stirred micro bench top reactor in semi-batch mode (continuous gas flow and liquid batch). The operation of the system is similar to the one used in the hydrogenation reactions. The conditions chosen for these reactions were 80 °C and 1.38 MPa with continuous bubbling of air (200 sccm). For the reaction in the emulsion phase, an emulsion with deionized water and tetralin was produced upon sonication with a Horn sonicator. In this reaction, the total liquid volume was 20 mL, at a water/tetralin ratio of 1:1 v/v. For the single-phase reaction, the total volume of tetralin was kept at 20 mL. The amount of catalyst in each reaction was 2 mg mL^{-1} with respect to tetralin.

The catalyst studied in these reactions was composed of 10 wt% Cu on MWCNT–Al_2O_3. It was prepared by incipient wetness impregnation of the support with an aqueous solution of the metal precursor ($Cu(NO_3)_3{\cdot}3\,H_2O$, provided by Sigma Aldrich). Then, the catalyst was dried overnight at 100 °C and calcined in air at 250 °C for 2 h.

Acknowledgements

Funding was provided by the Department of Energy (DE-SC0004600) and the Advanced Energy Consortium (AEC; BP America, Baker Hughes, ConocoPhillips, Halliburton, Marathon, Occidental, Petrobras, Schlumberger, Shell, and Total). The authors would also like to acknowledge the following people for their contributions in this work: Veronica M. Irurzun from the University of Oklahoma, Gregory W. Strout from the Samuel Roberts Noble Electron Microscopy Laboratory at the University of Oklahoma, and Terry Colberg from the Oklahoma State University Microscopy Laboratory.

Keywords: carbon nanotubes · hydrogenation · nanoparticles · oxidation · supported catalysts

[1] S. Iijima, *Nature* **1991**, *354*, 56 – 58.
[2] R. H. Baughman, A. A. Zakhidov, W. A. de Heer, *Science* **2002**, *297*, 787 – 792.
[3] Z. Wu, Z. Chen, X. Du, J. M. Logan, J. Sippel, M. Nikolou, *Science* **2004**, *305*, 1273 – 1276.
[4] E. Bekyarova, M. E. Itkis, N. Cabrera, B. Zhao, A. Yu, J. Gao, R. C. J. Haddon, *J. Am. Chem. Soc.* **2005**, *127*, 5990 – 5995.
[5] C. T. White, T. N. Todorov, *Nature* **1998**, *393*, 240 – 242.
[6] M. Zhang, S. Fang, A. A. Zakhidov, S. B. Lee, A. E. Aliev, C. D. Williams, K. R. Atkinson, R. H. Baughman, *Science* **2005**, *309*, 1215 – 1219.
[7] S. Iijima, C. Brabec, A. Maiti, J. Bernholc, *J. Chem. Phys.* **1996**, *104*, 2089 – 2092.
[8] V. K. Gupta, N. B. Pangannaya, *World Pat. Inf.* **2000**, *22*, 185 – 189.
[9] D. E. Resasco, W. E. Alvarez, F. Pompeo, L. Balzano, J. E. Herrera, B. Kitiyanan, A. Borgna, *J. Nanopart. Res.* **2002**, *4*, 131 – 136.
[10] E. T. Thostenson, Z. Ren, T. W. Chou, *Compos. Sci. Technol.* **2001**, *61*, 1899 – 1912.
[11] J. P. Salvetat, G. A. D. Briggs, J. M. Bonard, R. R. Bacsa, A. J. Kulik, T. T. Stöckli, *Phys. Res. Lett.* **1999**, *82*, 944 – 947.
[12] T. Rueckes K. Kim, E. Joselevich, G. Y. Tseng, C. L. Cheung, C. M. Lieber, *Science* **2000**, *289*, 94 – 97.
[13] Z. Yao, H. W. C. Postma, L. Balents, C. Dekker, *Nature* **1999**, *402*, 273 – 276.
[14] G. Che, B. B. Lakshmi, E. R. Fisher, C. R. Martin, *Nature* **1998**, *393*, 346 – 349.
[15] P. Serp, M. Corrias, P. Kalck, *Appl. Catal. A* **2003**, *253*, 337 – 358.
[16] J. P. Tessonnier, A. Villa, O. Majoulet, D. S. Su, R. Schlögl, *Angew. Chem.* **2009**, *121*, 6665; *Angew. Chem. Int. Ed.* **2009**, *48*, 6543 – 6546.
[17] J. Zhang, X. Liu, R. Blume, A. Zhang, R. Schlögl, D. S. Su, *Science* **2008**, *322*, 73 – 77.
[18] W. Zhang, J. K. Sprafke, M. Ma, E. Y. Tsui, S. A. Sydlik, G. C. Rutledge, T. M. Swager, *J. Am. Chem. Soc.* **2009**, *131*, 8446 – 8454.
[19] X. Yanga, X. Wanga, J. Qiu, *Appl. Catal. A* **2010**, *382*, 131 – 137.
[20] H. B. Zhang, X. L. Liang, X. Dong, H. Y. Li, G. D. Lin, *Catal. Surv. Asia* **2009**, *13*, 41 – 58.
[21] S. Crossley, J. Faria, M. Shen, D. E. Resasco, *Science* **2010**, *327*, 68 – 72.
[22] M. Shen, D. E. Resasco, *Langmuir* **2009**, *25*, 10843 – 10851.
[23] X. M. Li, D. Reinhoudt, M. Crego-Calama, *Chem. Soc. Rev.* **2007**, *36*, 1350 – 1368.
[24] L. Zhang, D. E. Resasco, *Langmuir* **2009**, *25*, 4792 – 4798.
[25] J. L. Bahr, E. T. Mickelson, M. J. Bronikowski, R. E. Smalley, J. M. Tour, *Chem. Commun.* **2001**, *2*, 193 – 194.
[26] H. Wang, E. K. Hobbie, *Langmuir* **2003**, *19*, 3091 – 3093.
[27] B. P. Binks, J. A. Rodrigues, *Angew. Chem.* **2005**, *117*, 445 – 448; *Angew. Chem. Int. Ed.* **2005**, *44*, 441 – 444.
[28] D. E. Tambe, M. M. Sharma, *Adv. Colloid Interface Sci.* **1994**, *52*, 1 – 63.
[29] J. R. Bragg, US Pat. 5,855,243, **1999**.
[30] F. Leal-Calderon, V. Schmitt, *Curr. Opin. Colloid Interface Sci.* **2008**, *13*, 217 – 227.
[31] B. P. Binks, C. P. Whitby, *Langmuir* **2004**, *20*, 1130 – 1137.

[32] C. M. Starks, *J. Am. Chem. Soc.* **1971**, *93*, 195 – 199.
[33] H. Lü, J. Gao, Z. Jiang, F. Jing, Y. Yang, G. Wang, C. Li, *J. Catal.* **2006**, *239*, 369 – 375.
[34] H. Lü, J. Gao, Z. Jiang, Y. Yang, B. Song, C. Li, *Chem. Commun.* **2007**, 150 – 152.
[35] H. Nur, S. Ikeda, B. Ohtani, *J. Catal.* **2001**, *204*, 402 – 408.
[36] J. Faria, M. P. Ruiz, D. E. Resasco, *Adv. Synth. Catal.* **2010**, *In press*.
[37] D. Ugarte, *Carbon* **1995**, *33*, 989 – 993.
[38] A. C. Dillon, M. Yudasaka, M. S. Dresselhaus, *J. Nanosci. Nanotechnol.* **2004**, *4*, 691 – 703.
[39] A. W. Musumeci, E. R. Waclawik, R. L. Frost, *Spectrochim. Acta A* **2008**, *71*, 140 – 142.
[40] Y. Kobayashi, D. Takagi, Y. Ueno, Y. Homma, *Phys. E (Amsterdam, Neth.)* **2004**, *24*, 26 – 31.
[41] S. M. Bachilo, L. Balzano, J. E. Herrera, F. Pompeo, D. E. Resasco, R. B. Weisman, *J. Am. Chem. Soc.* **2003**, *125*, 11186 – 11187.
[42] J. R. Simpson, J. A. Fagan, M. L. Becker, E. K. Hobbie, A. R. Hight Walker, *Carbon* **2009**, *47*, 3238 – 3241.
[43] P. Delhaes, M. Couzi, M. Trinquecoste, J. Dentzer, H. Hamidou, C. Vix-Guterl, *Carbon* **2006**, *44*, 3005 – 3013.
[44] T. Prasomsri , D. Shi, D. E. Resasco, *Chem. Phys. Lett.* **2010**, *497*, 103 – 107.
[45] L. Guan, K. Suenaga, S. Iijima, *Nano Lett.* **2008**, *8*, 459 – 462.
[46] G. Kresse, J. Furthmüller, *Phys. Rev. B* **1996**, *54*, 11169 – 11186.
[47] G. Kresse, J. Hafner, *Phys. Rev. B* **1994**, *49*, 14251 – 14269.
[48] G. Kresse, J. Hafner, *Phys. Rev. B* **1993**, *48*, 13115 – 13118.
[49] G. Kresse, J. Hafner, *Phys. Rev. B* **1993**, *47*, 558 – 561.
[50] G. Kresse, J. Furthmüller, *Comp. Mater. Sci.* **1996**, *6*, 15 – 50.
[51] B. P. Binks, S. O. Lumsdon, *Langmuir* **2001**, *17*, 4540 – 4547.
[52] B. P. Binks, J. Philip, J. A. Rodrigues, *Langmuir* **2005**, *21*, 3296 – 3302.
[53] B. P. Binks, *Curr. Opin. Colloid Interface Sci.* **2002**, *7*, 21 – 41.
[54] W. Zheng, J. Zhang, B. Zhu, R. Blume, Y. Zhang, K. Schlichte, *ChemSusChem* **2010**, *3*, 226 – 230.
[55] A. R. Beltramone, D. E. Resasco, W. E. Alvarez, T. V. Choudhary, *Ind. Eng. Chem. Res.* **2008**, *47*, 7161 – 7166.
[56] T. T. Pham, S. P. Crossley, T. Sooknoi, L. L. Lobban, D. E. Resasco, R. G. Mallinson, *Appl. Catal. A* **2010**, *379*, 135 – 140.
[57] F. X. Llabrés i Xamena, O. Casanova, R. Galiasso Tailleur, H. Garcia, A. Corma, *J. Catal.* **2008**, *255*, 220 – 227.
[58] M. Nowotny, L. N. Pedersen, U. Hanefeld, T. Maschmeyer, *Chem. Eur. J.* **2002**, *8*, 3724 – 3731.
[59] M. Martan, J. Manassen, D. Vopsi, *Tetrahedron* **1970**, *26*, 3815 – 3827.
[60] W. E. Alvarez, B. Kitiyanan, A. Borgna, D. E. Resasco, *Carbon* **2001**, *39*, 547 – 558.
[61] W. E. Alvarez, F. Pompeo, J. E. Herrera, L. Balzano, D. E. Resasco, *Chem. Mater.* **2002**, *14*, 1853 – 1858.
[62] B. Kitiyanan, W. E. Alvarez, J. H. Harwell, D. E. Resasco, *Chem. Phys. Lett.* **2000**, *317*, 497 – 503.
[63] H. Hu, P. Bhowmik, B. Zhao, M. A. Hamon, M. E. Itkis, R. C. Haddon, *Chem. Phys. Lett.* **2001**, *345*, 25 – 28.

Received: September 29, 2010
Published online on December 23, 2010

